Dynamics of a Sodium Heat Pipe Reforming Reactor

A prototype of a sodium heat pipe reactor for steam reforming processes has been developed and tested at energy levels up to 6 kW. Both experimental and model simulation data were obtained. Temperature profiles at nonflow and nonreaction flow conditions were used to adjust the parameters of the model, along with an intrinsic rate equation measured in a differential, bench-scale apparatus.

Very good agreement between experiment and model was found for approximately 50 runs under steady state reaction conditions covering a range of process variables. Advantages of the heat pipe as a reactor energy source were confirmed. These include isothermal wall temperatures, energy flux transformation, adjusted flux profiles, and rapid start-up. These measurements and computations have provided a model from which optimized configurations have been determined.

J. T. Richardson, S. A. Paripatyadar, J. C. Shen
Department of Chemical Engineering
University of Houston
University Park
Houston, TX 77004

Introduction

Reactors for highly endothermic reactions at high temperatures are often heat-transfer limited. This is especially true in the case of steam reforming of methane (Rostrup-Nielsen, 1983). Conventional reforming furnaces consist of hundreds of parallel reactor tubes, small in diameter to accommodate heat transfer. Heat is usually supplied by radiant gas burners positioned to optimize the flux profile down in the tubes. Although in principle this design is easily accomplished, severe problems arise as the catalyst deactivates at the front of the bed and the reaction is no longer fast enough to absorb energy. Overheating of both the catalyst and tube results. The effect on the tube is most severe, since small temperature increases at elevated temperatures lead to metal failure and the reactor ruptures. A solution to this problem is to operate the tube wall isothermally with the energy flux profile adjusted to match the demands of the endothermic reaction. Unfortunately, this has eluded reactor designers, in spite of many novel and ingeneous attempts.

A sodium heat pipe is a device admirably suited for this application. Figure 1 shows the essential features of the heat pipe. Sodium, contained in an evacuated tube, absorbs energy at the evaporator end through melting and vaporization. Vapor molecules diffuse at sonic velocities to the opposite end of the pipe, where condensation occurs through removal of energy. Liquid sodium flows back to the evaporator, either through the effect of gravity or capillary forces in a wick along the inner surface of the tube. The process is very similar to reflux evaporation-condensation (Chi, 1976).

Since sodium has a vapor pressure that varies from about 5 to 200 kPa in the temperature range 900 to 1,300 K, it is a suitable materials for most endothermic reactions. The amount of sodium is adjusted to the desired power levels. Heat pipes have the following advantages as energy sources for reactors:

1. *Isothermal surfaces.* Evaporation-condensation occurs at a constant temperature determined by the partial pressure of the sodium vapor, which in turn is regulated by the difference between energy input and output.

2. *Energy flux transformation.* By adjusting the ratio between the condensing and evaporating surfaces, the input energy flux may be adjusted down by any factor. This is a distinct advantage in the case of compact reactors where extremely high flux values are encountered; for example, in solar chemical energy transmission systems (Hildebrandt and Rose, 1985). Central or dish solar collectors deliver flux densities of over 1 $MW \cdot m^{-2}$, ten times more than most endothermic reactions absorb. The flux must be stepped down to match the reaction to avoid overheating of the tube walls.

3. *Variable flux profile.* Energy is removed where it is needed and the flux profile varies with location along the surface and with time. This is important when catalyst activity changes along the bed.

4. *Rapid start-up and shut-down response.* These devices respond very rapidly since there are no moving mechanical parts and no significant temperature differentials.

Conceptual designs of heat pipe-type reactors for steam reforming have been proposed in the patent literature (McCallister, 1982) and a model for exothermic or heat-removing appli-

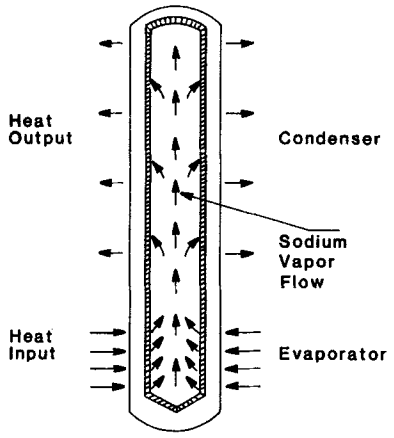

Figure 1. Details of sodium heat pipe.

cations discussed (Parent et al., 1983). However, to the authors' knowledge, no experimental demonstration has been reported.

This paper describes a prototype reactor for methane steam reforming using a sodium heat pipe. The research includes:

1. Demonstration of the concept with a commercial-size pilot unit
2. Development of a mathematical model for the reactor, properly calibrated with experimental data
3. Discussion of optimized designs for future applications

Experimental Method

Pilot unit

Figure 2 shows the flow diagram of the process supporting the reforming reactor. Natural gas from city pipelines is fed through a mass flow controller into the plant. After preheating, the gas is desulfurized in the zinc oxide reactor at 573–673 K in order to remove mercaptans. Steam is mixed with the desulfurized natural gas and the combined feed gas passes through a heat exchanger recovering heat from the product gas.

The reforming reactor is an enclosed shell with the heat pipe in the center. An infrared heater (Research Inc. model 4068-24-10) supplies radiant energy to the evaporator at up to 15–20 kW. After passing through heat exchangers, the product gas is further cooled with compressed air and quenched with water spray in the packed tower to condense unreacted steam. The compressed air transfers heat for the natural gas preheat. The cooled product gas is dried in silica gel drying columns and vented to the atmosphere through a venturi steam ejector at the top of a 12 m tower.

Stream gases are sampled prior to mixing with steam, after the reactor, after final drying and before venting. Analyses are made with an on-line Perkin-Elmer Sigma 1B gas chromatograph and Sigma 115 console. Methane, carbon monoxide, carbon dioxide, and hydrogen are measured directly; water is determined by material balance.

The unit is designed to operate at up to 20 kW input, methane feed rates up to 10 mol/min, steam to methane ratios from 0 to 5, and pressures up to 300 kPa. However, the infrared heater was found to be limited to efficiencies of less than 40%. This, together with unknown losses in piping, flanges, etc., restricts measured power levels (reaction, sensible, and insulation losses) to about 6 kW. Methane flow rates must be reduced accordingly in order to keep the reaction zone at the front of the bed where thermocouples are concentrated.

A MACSYM 2 minicomputer controls process flows, temperatures, pressures, and energy levels. The same system is used for data acquisition and processing. These include unit temperatures, temperature profiles in the reactor, and gas stream compositions.

Reactor

Details of the heat pipe reactor are shown in Figure 3. The outer shell of the reactor consists of a 15.2 cm ID pipe of schedule 40 Inconel with an overall length of 2.13 m. The heat pipe, 5.1 cm in dia., is situated along the center of the shell, leaving an annular space 5.1 cm thick and 1.83 m long for the catalyst bed.

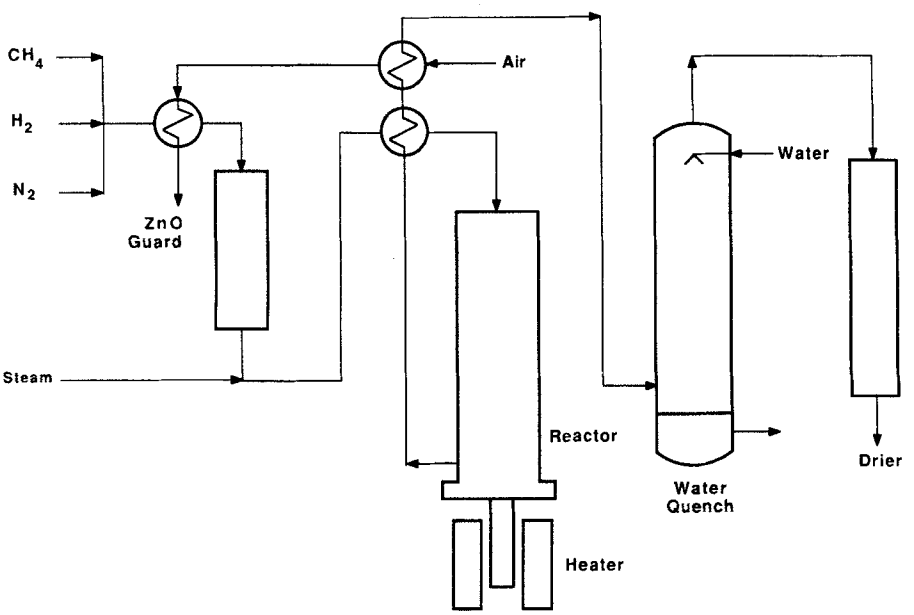

Figure 2. Process plant for methane reformer.

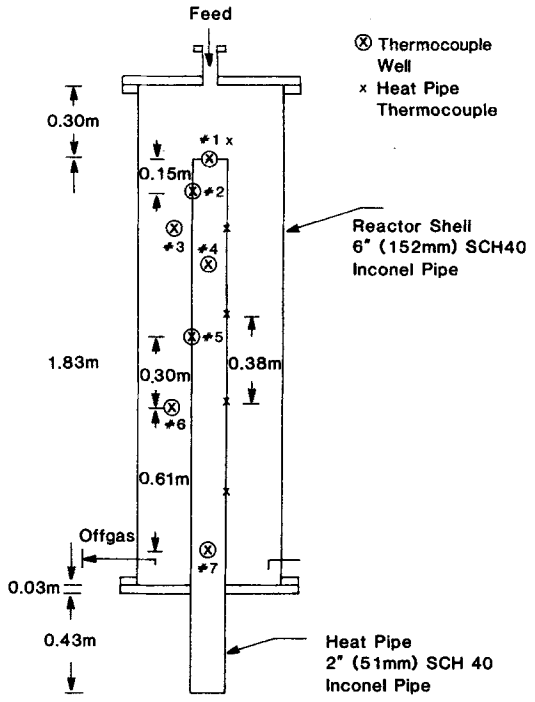

Figure 3. Heat pipe reactor.

The section above the heat pipe, 30.5 cm long, serves as a preheat region. An Inconel flange welded to the heat pipe forms the reactor bottom and is bolted to the outer shell with an Inconel-jacketed grafoil gasket.

Seven thermocouple wells are welded to the reactor outer shell in a 30° helical pattern. Each thermocouple well has four 3.2 mm Inconel-sheathed chromel-alumel thermocouples, spaced 3.2, 12.7, 22.2, and 31.8 mm from the heat pipe wall. Five thermocouples are also welded along the heat pipe, as shown in Figure 3. This arrangement of thermocouples provides a detailed measure of axial and radial temperature profiles, with a greater concentration at the front of the bed where greater gradients are expected.

The Inconel heat pipe was fabricated by the Dynatherm Corp., Baltimore, MD. The pipe was sealed, evacuated, and loaded with the required amount of sodium. The flange is positioned to provide an evaporator section 25 cm long. The condensing section contains a wick for the return flow of liquid sodium, even though the device is designed to operate vertically. This wick consists of four helical gutters 3.2 mm wide, made from stainless steel screen. Each gutter spirals about five times. Two layers of bias-cut screen provide a circumferential wick in the evaporator. The first layer, a 100-mesh stainless screen, is for good liquid distribution; the second, a layer of 325-mesh screen, inhibits nucleate boiling.

Dynatherm tested the heat pipe with an induction heat source and a water-cooled gas-gap calorimeter, confirming satisfactory operation at 15 kW in the temperature range 825 to 1,225 K. Under these conditions, the evaporator and condenser sections of the heat pipe have flux densities of 500 and 68 kW · m^{-2}, respectively.

The reactor exterior is insulated with a 12.7 cm thick layer of carborundum Fiberfrax Durablanket S-96, which gives an outside surface temperature of 338 K when the wall is at 922 K.

Table 1. Physical Properties of Topsoe RKG-2

Composition	14% Ni/Al_2O_3
Silica	<0.1%
Sulfur	<100 ppm
Crush strength	
Axial	400 kg · cm^{-2}
Radial	45 kg · cm^{-2}
BET surface area	20–30 $m^2 \cdot g^{-1}$
Pellet density	2,509 kg · m^{-3}
Sulfur capacity	1,000–1,500 ppm

Reforming catalyst

The catalyst, Haldor Topsoe RKG-2, is an industrial catalyst for steam reforming natural gas and naphtha. It is suitable for high-temperature reforming applications and has a high sulfur-tolerance. The pellets are ring-shaped with 12 mm OD, 5 mm ID, and 6 mm height, giving an equivalent diameter of 6.63 mm. Other properties are given in Table 1.

Received in the oxidized condition, the catalyst was reduced by the feed with steam/gas ratios from 6 to 8 and temperatures above 873 K.

The catalyst was loaded from the top into the reactor until the bed was level with the bottom of thermocouple well no. 7. The thermocouple assembly was then inserted into the well and bolted in place. Filling continued in this manner until the bed was level with the bottom of well no. 2. Space at the top of the heat pipe was left empty. This loading procedure required 30.7 kg of catalyst, giving a bed void fraction of 0.55 and a bulk density of 1,129 kg · m^{-3}.

Kinetic bench unit

A kinetic bench unit was used to measure the intrinsic kinetics of the powdered catalyst, and to compare the activity of the used catalyst taken from different bed locations against that of the fresh catalyst. The reactor was fabricated from a stainless steel tube (38.5 cm length, 6.35 mm dia.) equipped with Swagelok fittings to accommodate 1.6 mm dia. Inconel-sheathed, type K thermocouple. Up to 100 mg of catalyst particles (35–45 mesh) were mixed with alumina particles of similar size to form a bed approximately 1 cm^3 in volume. Methane and hydrogen were mixed in desired proportions using Tylan Mass Flow Controllers, preheated, and combined with vaporized water supplied by a Sage Instruments model 220 Syringe Pump through a boiler. The feed was preheated to reaction temperatures between 823 and 973 K and at atmospheric pressure and then passed through the bed at sufficient velocity to avoid diffusion limitations and assure differential operation with less than 5% conversion. The product gas was dried and analyzed with the same system used in the pilot unit operations. Feed compositions and temperatures were varied over a wide range. Differential rates were measured for a period of several hours and extrapolated back to zero time in order to account for any deactivation. Initial rates were then examined in the usual way to determine the kinetics of the forward reactions.

Simulation Model

Steam reforming of methane is a combination of two reactions:

$$CH_4 + H_2O = CO + 3H_2 \qquad (1)$$

$$CO + H_2O = CO_2 + H_2 \quad (2)$$

with equilibrium constants K_R and K_S, respectively. Other reactions, which produce and remove carbon, occur (Rostrup-Nielsen, 1983), but these are not included in the model since their rates are small compared to those of the main reactions. It is assumed that Eq. 2 is always at equilibrium, an assumption justified in later discussion. The reaction rate R is then determined by the kinetics of Eq. 1.

Axial dispersion in the reactor is neglected, so that the equations for a two-dimensional pseudohomogeneous model are:

Material balance:

$$\frac{\partial x}{\partial z} - \frac{d_p}{Pe_r}\left(\frac{\partial^2 x}{\partial r^2} + \frac{1}{r}\frac{\partial x}{\partial r}\right) - \frac{(R\,\rho_B \eta)}{G^o_{CH_4}} = 0 \quad (3)$$

with boundary conditions

$$x = x_{in} \quad \text{at} \quad z = 0 \quad (4)$$

$$\left(\frac{\partial x}{\partial r}\right) = 0 \quad \text{at} \quad r = R_{HP}, \quad z > 0 \quad (5)$$

$$\left(\frac{\partial x}{\partial r}\right) = 0 \quad \text{at} \quad r = R_W, \quad z > 0 \quad (6)$$

Energy balance:

$$G_T Cp_m \frac{\partial T}{\partial z} - k_{er}\left(\frac{\partial^2 T}{\partial r^2} + \frac{1}{r}\frac{\partial T}{\partial r}\right) - R\,\rho_B \eta(-\Delta H_R) = 0 \quad (7)$$

with boundary conditions

$$T = T_{in} \quad \text{at} \quad z = 0 \quad (8)$$

$$\left(-k_{er}\frac{\partial T}{\partial r}\right)_{r=R_{HP}} = U_{HP}\,(T_{HP} - T_o), \quad z > 0 \quad (9)$$

$$\left(-k_{er}\frac{\partial T}{\partial r}\right)_{r=R_W} = U_W(T_{NR} - T_a), \quad z > 0 \quad (10)$$

Pressure terms are not used since the pressure drop is negligible at the flow rates used in these experiments.

Pseudohomogeneous models assume that the solid-fluid system is a single phase through which heat transfer in the radial direction is by conduction only. Kulkarni and Doraiawamy (1980) reviewed various correlations available in the literature for the effective thermal conductivity, k_{er}, in the radial direction of the packed bed. Several of these were tested and the most effective was found to be the parallel-series model of Argo and Smith (1953), which assumes radial conduction, radiation, and convection to be parallel and series in the fluid and solid phases, respectively. This gives

$$k_{er} = \delta(k_c + k_{cv} + k_r) + (1 - \delta)k_{series} \quad (11)$$

in which k_c, the conductivity of the fluid phase, is given by

$$k_c = k_m \quad (12)$$

and

$$k_{cv} = G_T Cp_m d_p/(\delta\, Pe_r) \quad (13)$$

$$k_r = 2.29 \times 10^{-11}\, d_p \frac{\epsilon_s}{(2 - \epsilon_s)} T^3 \quad (14)$$

The conductivity of the solid phase, k_{series}, is found from

$$k_{series} = \frac{h\, k_s\, d_p}{2k_s + hd_p} \quad (15)$$

where

$$h = h_c + h_{cv} + h_r \quad (16)$$

$$h_c = k_p(2k_s + hd_p)/(d_p k_s) \quad (17)$$

$$k_p = 10^{(-3.52 + 0.745 k_s/\delta)} \quad (18)$$

$$h_{cv} = 1.95\, G_T Cp_m Re_p^{-0.51}/Pr^{2/3}, \; Re_p < 350$$
$$= 1.06\, G_T Cp_m Re_p^{-0.41}/Pr^{2/3}, \; Re_p > 350 \quad (19)$$

$$h_r = k_r\,(2k_s + hd_p)/(d_p k_s) \quad (20)$$

$$Pr = Cp_m \mu_m / k_m \quad (21)$$

$$Re_p = G_T d_p/\mu_m \quad (22)$$

$$Pe_r = 9.0\left[1 + 19.4\left(\frac{d_p}{d_t}\right)^2\right] \quad (23)$$

with

$$d_t = 2(R_W - R_{HP}) \quad (24)$$

Neglecting conduction, the overall heat transfer coefficient at the heat pipe wall, U_{HP}, is given by

$$U_{HP} \simeq (h_{cv} + h_r)_{HP} \quad (25)$$

It was assumed that the radiated energy from the heat pipe is absorbed by the first catalyst layer so that

$$(h_r)_{HP} = F_{12}\,\sigma\left(\frac{T_{HP}^4 - T_o^4}{T_{HP} - T_o}\right) \quad (26)$$

where the geometric factor, F_{12}, is given by

$$F_{12} = \frac{1}{\left(\frac{1}{\epsilon_{HP}} + \frac{1}{\epsilon_s} - 1\right)} \quad (27)$$

For the convective heat transfer coefficient, h_{cv}, two separate cases were considered. When there is no reaction

$$(h_{cv})_{HP} = 1.34 \times 10^{-6}\, Re_p\left(\frac{d_t}{d_p}\right) \quad (28)$$

For the case with reaction, the correlation of Chao et al. (1973)

gives

$$(h_{cv})_{HP} = 0.39 \frac{k_m}{d_p} Re_p^{0.6} \tag{29}$$

At the reactor wall, the overall heat transfer coefficient includes the wall heat transfer coefficient h_w, conduction through the reactor wall and insulation, and the outside heat transfer coefficient for heat loss to the surroundings, h_o. This results in

$$\frac{1}{U_W} = \frac{1}{h_w} + \frac{R_W \ln (R_2/R_W)}{k_w} + \frac{R_W \ln (R_3/R_W)}{k_{ins}} + \frac{R_W}{R_3 h_o} \tag{30}$$

where

$$R_2 = R_W + t_w \tag{31}$$

$$R_3 = R_2 + t_{ins} \tag{32}$$

$$h_w \simeq (h_r + h_{cv})_W \tag{33}$$

$$(h_r)_W = F_{12}\, \sigma \left(\frac{T_{NR}^4 - T_W^4}{T_{NR} - T_W} \right) \tag{34}$$

$$F_{12} = \frac{1}{\left(\frac{1}{\epsilon_W} + \frac{1}{\epsilon_s} - 1 \right)} \tag{35}$$

and $(h_{cv})_W$ is given by Eqs. 28 and 29.

For the outside heat transfer coefficient h_o,

$$h_o = (h_r)_{ins} + h_{ncv} \tag{36}$$

where

$$(h_r)_{ins} = 0.9\, \sigma \left(\frac{T_{ins}^4 - T_a^4}{T_{ins} - T_a} \right) \tag{37}$$

and the natural convection heat transfer coefficient h_{ncv} is calculated from the correlations given by McCabe and Smith (1985).

The intrinsic rate R was found from a rate equation determined experimentally with the laboratory kinetic unit. Details are given in later discussion. For the calculation of the effectiveness factor η, a generalized Thiele modulus ϕ was used as follows

$$\phi = \frac{V_p}{S_x} \frac{R(C_{CH_4}^s)\, \rho_p}{(2\, D_e)^{1/2}} \left[\int_{C_{CH_4}^{eq}}^{C_{CH_4}^s} R\, \rho_p\, dC_{CH_4} \right]^{-1/2} \tag{38}$$

giving

$$\eta = \frac{3\phi \coth (3\phi) - 1}{3\phi^2} \tag{39}$$

Effective diffusivities were calculated using the same procedures as De Deken et al. (1982).

These equations were transformed into second-order finite-difference equations for improved accuracy. Solutions were found using Fortran 77 programming with a National Advance System AS/9000. A radial step size of 3.11×10^{-3} m was used to match thermocouple positions. A value of 1.27×10^{-4} m was sufficient for the axial step size. Average axial temperatures were calculated from both the simulation and experimental axial values using an area-weighted expression.

A one-dimensional model was also developed by assuming a constant average temperature across the bed. Mass and energy balance equations were modified accordingly so that a simpler set of differential equations could be solved with fewer increments and iterations. The program was written in Basic and executed on an IBM XT computer. Although not as accurate and informative as the two-dimensional model, this simulation was useful for rapid scoping studies.

Results and Discussion

Intrinsic kinetics

Intrinsic kinetics were studied at atmospheric pressure, five temperatures between 800 and 950 K, and steam to methane ratios between 2.5 and 5. In three sets of experiments, the hydrogen to methane ratio was 0.5, 1.0, and 2.0 respectively. Fresh catalyst samples were used for different temperatures and each run was completed in 5 h, with rates extrapolated back to zero time. Initial conditions were checked at the end of all experiments at a given temperature. A slight irreversible deactivation (less than 10%) was found that could not be identified. No carbon formation was observed, so it was concluded that loss of activity was either due to sintering or, most likely, deposition of poisons, such as silica, from the feed stream. In order to correct for the deactivation, a linear decay rate was assumed and all initial rates adjusted accordingly.

Previous studies by Akers and Camp (1955) showed excellent agreement with first-order kinetics. In a recent review, Van Hook (1980) concluded that first order adequately describes most available data, although De Deken et al. (1982) report Langmuir-Hinshelwood rate expressions. In this work, 30 data sets covering five temperatures correlated with the rate equation

$$R = 8.82 \times 10^{-2}\, e^{(-53{,}326/RgT)}\, P_{CH_4} \text{mol/s} \cdot \text{g cat} \tag{40}$$

with a regression coefficient of 0.969, sufficiently accurate for the purpose here.

Equation 40 was modified to account for the reverse reaction

$$R = k\, P_{CH_4} \left(1 - \frac{P_{CO} P_{H_2}^3}{P_{CH_4} P_{H_2O} K_R} \right) \text{mol/s} \cdot \text{g cat} \tag{41}$$

and used in the model computations.

Product distributions were compared with equilibrium calculations and it was found that, even at these low conversions, shift equilibrium is attained below 875 K and approaches 80–90% for higher temperatures. Under process conditions, the assumption of shift equilibrium appears to be justified.

Heat transfer parameter estimation

Heat transfer parameters in the simulation model were estimated from correlations reported in the literature. These correlations were obtained over a wide range of conditions, usually nonreactive, and for particle geometries different from the

RKG-2 rings. Since these parameters are critical in predicting performance of a heat transfer limited reactor, it is necessary to confirm or correct the estimated values with appropriate experiments. For this purpose, two types of measurements were made. The first involved nonflow conditions, the second flow but nonreaction. Thus, conduction and radiation could be examined independently from convection.

Nonflow Experiments. Four pilot unit runs were made with the catalyst bed blanketed with nitrogen and no flow through the reactor. Assuming minimal losses at the top and bottom of the reactor, steady state temperature profiles should reflect radial energy flow from the heat pipe out through the bed, reactor wall, and insulation into the environment. Table 2 gives typical temperature profiles for one of these runs. The data in Table 2 show temperature gradients in the radial direction. Interpolated values at the surface of the heat pipe are almost constant and agree with the evaporator temperature after allowing for the small temperature differentials in the evaporator and condenser walls (<10 and 1 K, respectively). Effective thermal conductivity k_{er}, and the overall heat transfer coefficient U_{HP}, for nonflow conditions were estimated from these results in the following manner.

Under nonflow conditions, the energy balance equation reduces to

$$\frac{1}{r}\frac{\partial}{\partial r}(rq_r) = 0 \tag{42}$$

Substituting for q_r,

$$\frac{\partial}{\partial r}\left(-rk^o_{er}\frac{\partial T}{\partial r}\right) = 0 \tag{43}$$

or

$$-rk^o_{er}\frac{\partial T}{\partial r} = \text{constant} = q_L R_W \tag{44}$$

where q_L is the heat loss flux at the reactor wall, calculated with the simulation model.

This procedure was followed for four sets of profiles and the measured values of k_{er} compared with those calculated with the model. This comparison is shown in Figure 4.

Over the temperature range covered, the model could be adjusted to agree with experimental values by multiplying the radiation term k_r in Eq. 14 by the correction factor

$$f_c = -3.04 + 5.92 \times 10^{-3}\,T - 2.36 \times 10^{-6}\,T^2 \tag{45}$$

Table 2. Radial Temperature Profile, Nonflow Conditions

Axial Position m	Temperature, K, at Radial Position from Heat Pipe, cm				
	0*	0.32	1.27	2.22	3.18
0.15	1,122	1,116	1,090	1,058	1,037
0.30	1,124	1.123	1,101	1,077	1,064
0.61	1,123	1,122	1,102	1,083	1,068
1.52	1,133	1,132	1,100	1,090	1,074

Power input, 0.853 kW; heat pipe evaporator temp., 1,134 K
*Interpolated values

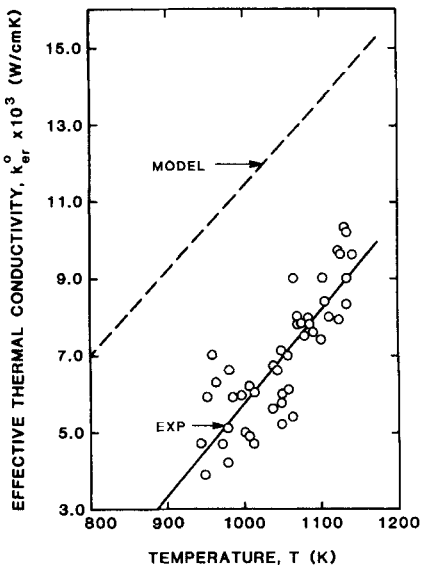

Figure 4. Experimental and predicted k_{er}.

Calculated values of U_{HP} were found to be within 5% of those measured, so that no correction to the correlation was necessary.

Nonreactive Flow Experiments. The next step was to obtain temperature profiles under flow conditions without chemical reaction and verify convective heat transfer correlations and parameters estimated from nonflow data. Different steam flow rates and heat pipe temperatures were used in a series of runs. A small flow of hydrogen (about 5 vol. %) was maintained to prevent oxidation of the catalyst and sintering due to high-temperature steaming. Figure 5 shows typical radial and average axial temperature profiles for one of these runs.

Simulation model results, also shown in Figure 5, are in very good agreement with measured values, with differences not exceeding 10 K, well within experimental error and the assumptions of the model. Enthalpy changes, measured and predicted, agree to within 3%. These results indicate that the heat transfer correlations used in the model together with the correction factor given by Eq. 45 are adequate to predict heat transfer in the reactor.

Steam reforming experiments

Catalyst Deactivation Tests. The heat pipe reactor was tested in a series of 51 experiments covering a wide range of process variables under steady state conditions. Thirty-nine of these were part of a study simulating daily solar cycles to be reported elsewhere (Paripatyadar and Richardson). At the conclusion of all experiments, the catalyst was withdrawn from the unit in segments of depth and tested in the laboratory unit under standard conditions (T = 863 K, H_2O/CH_4 = 5, H_2/CH_4 = 1). Compared to the fresh catalyst, the activity declined by a factor of 0.078. This was believed to be a consequence of a mishap in the early stages in which the catalyst was steamed at elevated temperatures without methane or hydrogen. Accordingly, a factor of 0.078 was applied to the preexponential factor of Eq. 41 in all subsequent simulation calculations.

Steady State Reaction Performance. Process condition ranges for the steady state experiments are given in Table 3. Full

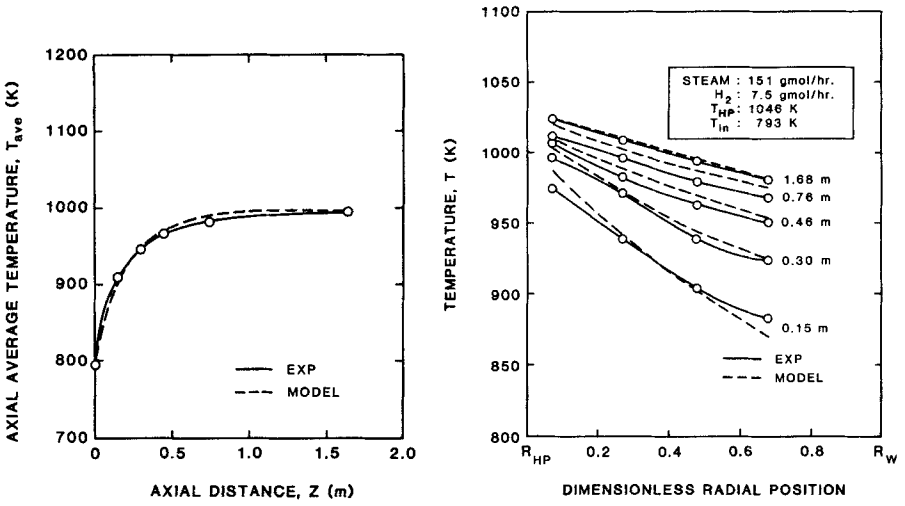

Figure 5. Radial and average temperature profiles for flow conditions without reaction.

Table 3. Process Condition Ranges for Steady State Experiments

CH_4 flow, mol/h	23–102
H_2O/CH_4 ratio	2.3–7.4
Pressure, kPa	130–238
T_{HP}, K	952–1,100
T_{in}, K	493–727
Power, kW	2.42–6.10

details of these experiments are given by Shen (1984) and Paripatyadar (1987). Typical results are shown in Figures 6 and 7 for two runs with different heat pipe temperatures. Differences in axial positions for the thermocouple sets are due to the addition of fresh catalyst to the top of the bed between the runs. Measured axial temperatures are in excellent agreement with the model, differing only by 10 K. Radial temperatures are also very close.

Exit gas compositions, given in Table 4, also agree well with model predictions. The agreement is less for the high conversion at 1,043 K, especially for methane concentration. This may be due to imprecision in the analysis at this low level. Nevertheless, the values are within the expectations of the model accuracy. Additional details for the run shown in Figure 6 are given in Table 5, including average axial temperatures from both the two- and one-dimensional models, and calculated conversions and flux densities.

Table 5 shows several features that demonstrate the dynamics of the heat pipe reactor. First, the condensing surface of the heat pipe, the source of energy to the catalyst bed, is close to isothermal and is smaller than the evaporator temperature by about 13–15 K. This is consistent with expected gradients in the heat pipe wall for the flux levels used. Second, calculated flux densities at the heat pipe are greatest at the front of the bed, where rates are the highest, and decrease along the bed as rates fall with approach to equilibrium. Note, however, that the heat pipe wall remains at the same temperature. The flux values are low. This is because flow rates and Reynolds numbers are much lower than those found in commercial applications. Heat transfer is predominantly radiative and convection adds only a small part. At higher velocities, it is expected that the usual flux values of about 50–60 kW m^{-2} would be attained easily.

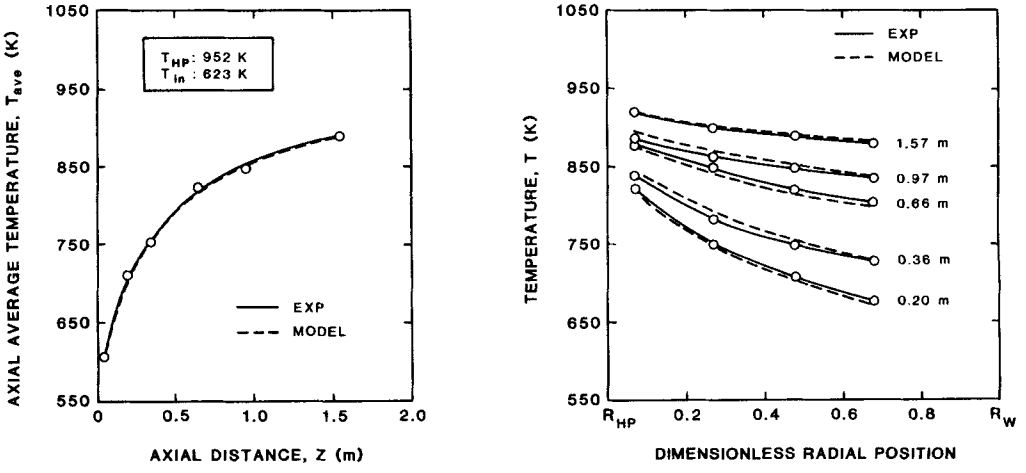

Figure 6. Axial and radial temperature profiles.

T_{HP} = 952 K; CH_4 flow = 40.8 mol/h; H_2O/CH_4 = 2.79; P_T = 131 kPa; power = 2.34 kW

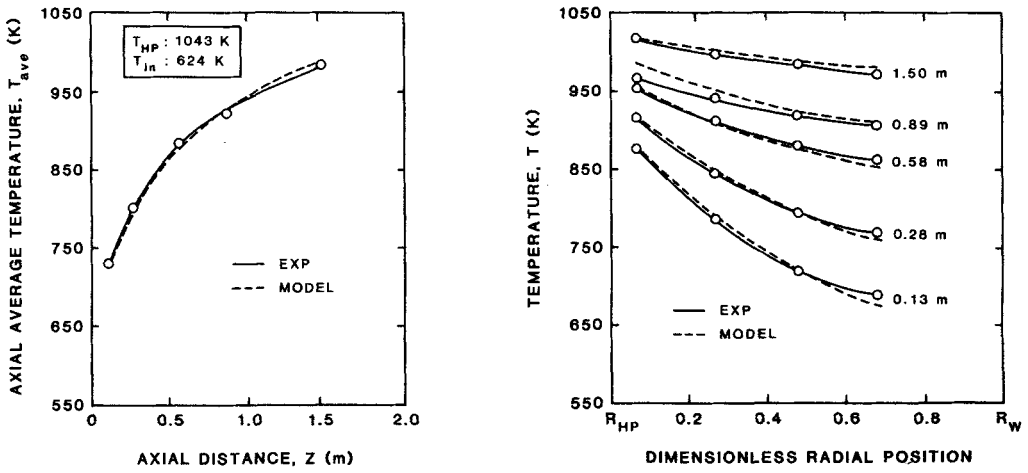

Figure 7. Axial and radial temperature profiles.
T_{HP} = 1,043 K; CH_4 flow = 47.7 mol/h; H_2O/CH_4 = 2.64; P_T = 132 kPa; power = 3.07 kW

Third, there are severe temperature gradients in the bed. This is seen both in the average temperatures in Table 5 and in the profiles of Figures 6 and 7. The largest gradients are close to the heat pipe due to the low flow rates. Once again, higher convection for industrial conditions will lessen this problem.

Table 5 also affirms the good agreement between experiment and simulation for both the one- and two-dimensional models. These models may now be used with confidence in future studies of different conditions and reactor configurations, the one-dimensional model for rapid screening and parametric investigations, and the two-dimensional model for more detailed design.

The heat pipe reactor performed with this degree of confidence for all 51 runs, covering an operating period of 600 h. No deterioration of catalyst or heat pipe was encountered. The only problem was due to hydrogen permeation into the heat pipe, discussed next.

Hydrogen Permeation. Hydrogen permeation into the heat pipe was discovered during the first reduction of the catalyst, using dry hydrogen. As the reduction progressed, the temperature at the top of the heat pipe decreased and the cold zone moved continuously down the pipe. It soon became apparent that hydrogen was permeating through the wall of the heat pipe, forming a gas pocket at the top and preventing the sodium vapor from transferring heat to the upper section. After 19 h the heat pipe condenser volume was completely filled with hydrogen.

Hydrogen permeation was confirmed by reversing the process. With nitrogen in the reactor, the heat pipe was heated and hydrogen diffused out. Expelling hydrogen was a slow process since only at the interface of the sodium vapor and hydrogen was the temperature high enough to have a significant permeation rate. By using heating cycles in which the temperature was raised for 1 h then lowered for 3 h so that the hydrogen bubble expanded, the available hot surface for reverse permeation was increased. Nevertheless, this recovery process took 28 days to complete.

Studies of hydrogen permeation in Incoloy 800 indicated that the permeation rate at 800 K is 3.1×10^2 cm^3 · m^{-2} · h^{-1} for pure hydrogen (Kugeler et al., 1970). The rate experienced here was about five times this value, which is not unreasonable for Inconel 600. However, the same studies showed that in the presence of at least equal amounts of steam, the oxidized metal surface reduces the rate to 1.7×10^{-2} cm^3 · m^{-2} · h^{-1}, a factor of four orders of magnitude. It seemed reasonable, therefore, that permeation would not be so much of a problem in normal steam reforming atmospheres. In subsequent runs, the catalyst was reduced with the feed gas and normal operations showed only minor amounts of hydrogen permeation, which could be controlled by reverse heating as described. A more permanent solution would be to utilize a permeation seal that preferentially lets hydrogen but not sodium vapor pass, or to vacuum periodically when operations permit. Figure 8 demonstrates the effect of hydrogen permeation. At the top of the heat pipe, the measured temperature is over 100 K below that expected. Clearly, the

Table 4. Carbon Compositions of Product Gases

T_{HP} K		Product Composition, C% CO	CH_4	CO_2	Conversion x
952	Exper.	33.4	21.0	45.5	0.790
	Model	33.1	22.7	44.1	0.773
	Equilib.	33.2	22.6	44.2	0.774
1,043	Exper.	61.3	2.4	36.4	0.976
	Model	60.4	4.4	35.2	0.956
	Equilib.	59.3	5.0	35.7	0.950

Table 5. Typical Axial Profiles

z m	Heat Pipe Temp.* K	Avg. Temp., K Meas.	Model 2-D	Model 1-D	Conversion** x	Q** kW · m^{-2}
0.05	936	606	606	605	0.098	16.1
0.20	937	710	716	704	0.229	12.3
0.36	937	754	755	764	0.333	10.4
0.66	938	823	816	838	0.501	7.7
0.97	938	845	850	873	0.617	5.8
1.57	939	886	885	893	0.754	3.6

T_{HP} = 952 K; CH_4 flow = 40.8 mol · h^{-1}; H_2O/CH_4 = 2.79
P_T = 131 kPa; power = 2.34 kW
*Interpolated; **2-D model

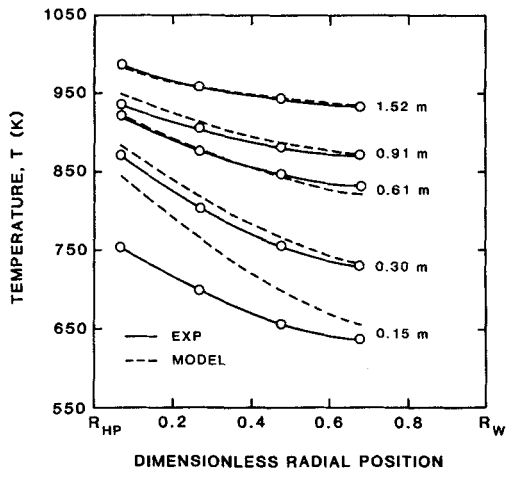

Figure 8. Effect of hydrogen permeation on radial temperature profiles.

sodium is not operating and the wall temperature is produced by conduction from the lower part of the heat pipe. Nevertheless, it is interesting how the heat pipe "recovers" by extracting heat as the reaction accelerates in the lower part of the bed. At the exit, the temperature and conversion is consistent with model values.

Heat Pipe Reactor Assessment and Optimization

The results of these experiments confirm the potential of the heat pipe reactor for heat-transfer limited, endothermic processes. Heat pipe temperatures are indeed isothermal after allowing for expected temperature gradients in the wall. These were never more than 15 K at the evaporator and 1 K at the condenser under the conditions tested here. Higher fluxes will result in greater gradients at the evaporator, but the benefits of the heat pipe characteristics more than compensate for this. Isothermal operation is confirmed by both measurements and agreement with the model based on this assumption.

Flux density transformation is evident in these data. High incident flux densities can be accommodated, reduced, and transmitted to the reaction without the catastrophic tube heating encountered in conventional reformers. There are other advantages. Not only is it unnecessary to match the flux profile to catalyst activity, but deactivation of the catalyst at the top of the tube is no problem since the reaction zone merely shifts and heat withdrawal adjusts to meet the need. Although not tested directly, this feature is evident from the characteristics of the heat pipe and predicted performance from the simulation.

Response is very fast. In these experiments, the bed could be heated to process conditions in several hours. Exact times depend upon the heat capacity of the bed, but the critical factor is the heating rate of the pipe, recommended by the manufacturer to be no greater than 1.4 kW/min.

The configuration of this heat pipe reactor, although well suited for these types of measurements, is not satisfactory for actual process applications. There is too much loss from the outer wall, radial gradients are too large, and heat transfer surfaces are small. However, with the calibrated simulation model, consideration of better arrangements is now possible.

Acknowledgment

This work was funded in part by the Department of Energy and the Solar Energy Research Institute, Contract No. DE-ACO3-81SF-1155, and the Energy Laboratory of the University of Houston. We are grateful to George Hadjigeorghiou and Josianne Ginestra for collaboration during critical stages of the work.

Notation

$C^{eq}_{CH_4}$ = concentration of methane at equilibrium, gmol · cm^{-3}
$C^{s}_{CH_4}$ = concentration of methane at pellet surface, gmol · cm^{-3}
Cp_m = heat capacity of gas mixture, J · gmol^{-1} · K^{-1}
d_p = equivalent diameter of particle, cm
d_t = equivalent diameter of reactor, cm
D_e = effective diffusivity, cm^2 · s^{-1}
f_c = correction factor for radiation
F_{12} = geometric factor for radiation
$G^{o}_{CH_4}$ = inlet molar flux of methane, gmol · cm^{-2} · s^{-1}
G_T = total molar flux, gmol · cm^{-2} · s^{-1}
h = heat transfer coefficient, solid phase, W · cm^{-2} · K^{-1}
h_c = heat transfer coefficient, conduction, W · cm^{-2} · K^{-1}
h_{cv} = heat transfer coefficient, convection, W · cm^{-2} · K^{-1}
$(h_{cv})_{HP}$ = heat transfer coefficient, convection at heat pipe, W · cm^{-2} · K^{-1}
$(h_{cv})_W$ = heat transfer coefficient, convection at reactor wall, W · cm^{-2} · K^{-1}
h_r = heat transfer coefficient, radiation, W · cm^{-2} · K^{-1}
$(h_r)_{HP}$ = heat transfer coefficient, radiation at heat pipe, W · cm^{-2} · K^{-1}
$(h_r)_W$ = heat transfer coefficient, radiation at reactor wall, W · cm^{-2} · K^{-1}
$(hr)_{ins}$ = heat transfer coefficient, radiation from outer insulation, W · cm^{-2} · K^{-1}
h_w = heat transfer coefficient, inner wall, W · cm^{-2} · K^{-1}
h_o = heat transfer coefficient, to surroundings, W · cm^{-2} · K^{-1}
h_{ncv} = heat transfer coefficient, natural convection, W · cm^{-2} · K^{-1}
ΔH_R = heat of reaction, J/gmol
k = rate constant for steam reforming, gmol · s^{-1} · (g cat)$^{-1}$ · (kPa)$^{-1}$
k_c = thermal conductivity, conduction, W · cm^{-1} · K^{-1}
k_m = thermal conductivity, gas mixture, W · cm^{-1} · K^{-1}
k_{cv} = thermal conductivity, convection, W · cm^{-1} · K^{-1}
k_r = thermal conductivity, radiation, W · cm^{-1} · K^{-1}
k_s = thermal conductivity, solid, W · cm^{-1} · K^{-1}
k_{series} = thermal conductivity of series mechanism in solid phase, W · cm^{-1} · K^{-1}
k_p = thermal conductivity, pellet, W · cm^{-1} · K^{-1}
k_w = thermal conductivity, inconel, W · cm^{-1} · K^{-1}
k_{ins} = thermal conductivity, insulation, W · cm^{-1} · K^{-1}
k_{er} = effective thermal conductivity, W · cm^{-1} · K^{-1}
k^{o}_{er} = effective thermal conductivity, nonflow, W · cm^{-1} · K^{-1}
K_R = equilibrium constant for steam reforming, kPa^2
K_S = equilibrium constant for water-gas shift reaction
P_C = partial pressure of component C, kPa
P_T = total pressure, kPa
Pe_r = radial Peclet number
Pr = Prandtl number
q_r = heat flux in radial direction, W · cm^{-2}
q_L = heat loss flux at reactor wall, W · cm^{-2}
Q = heat flux at heat pipe, W · cm^{-2}
r = radial dimension, cm
R = rate of steam reforming, gmol · s^{-1} · (g cat)$^{-1}$
Re_p = particle Reynolds number
Rg = gas constant, J · gmol^{-1} · K^{-1}
R_{HP} = radius of the heat pipe, cm
R_W = radius of the reactor inner wall, cm
S_g = internal surface area of catalyst pellet, cm^2 · g^{-1}
S_x = external surface area of pellet, cm^2
T = temperature, K
T_{in} = inlet temperature, K
T_{ave} = axial average temperature, K
T_a = temperature of environment, K
T_o = temperature of catalyst bed adjacent to heat pipe, K
T_{NR} = temperature of catalyst bed adjacent to reactor wall, K
T_{ins} = temperature of outer insulation, K
T_{HP} = heat pipe temperature, K
t_w = reactor wall thickness, cm
t_{ins} = insulation thickness, cm

U_{HP} = overall heat transfer coefficient at heat pipe, W · cm^{-2} · K^{-1}
U_W = overall heat transfer coefficient at reactor inner wall, W · cm^{-2} · K^{-1}
V_p = volume of pellet, cm^3
x = fractional conversion of methane in reforming reaction
x_{in} = inlet fractional conversion of methane
z = axial dimension, cm

Greek letters

δ = void fraction of bed, cm^3 void (cm^3 bed)$^{-1}$
ϵ_s = emissivity of catalyst
ϵ_{HP} = emissivity of heat pipe
η = effectiveness factor
μ_m = viscosity, gas mixture, g · cm^{-1} · s^{-1}
ρ_B = bulk density, g · cm^{-3} bed
ρ_P = pellet density, g · cm^{-3} pellet
σ = Boltzmann constant, W · cm^{-2} · K^{-4}
ϕ = Thiele modulus
ϵ_w = emissivity of reactor wall

Literature Cited

Akers, W. W., and D. P. Camp, "Kinetics of the Methane-Steam Reaction," *AIChE J.*, **1**(4), 471 (1955).

Argo, W. B., and J. M. Smith, "Heat Transfer in Packed Beds," *Chem. Eng. Prog.*, **49**(8), 443 (1953).

Chao, R. E., R. A. Caban, and M. M. Irizarry, "Wall Heat Transfer to Chemical Reactors," *Can. J. Chem. Eng.*, **51**, 67 (1973).

Chi, S. W., *Heat Pipe Theory and Practice*, McGraw-Hill, New York (1976).

De Deken, J. C., E. F. Devos, and G. F. Froment, "Steam Reforming of Natural Gas: Intrinsic Kinetics, Diffusional Influences, and Reactor Design," *Am. Chem. Soc. Symp. Ser.*, **196**, 181 (1982).

Hildebrandt, A. F., and K. A. Rose, "Receiver Design Considerations for Solar Central Receiver Hydrogen Production," *Solar Energy*, **35**, 199 (1985).

Kulkarni, B. D., and L. K. Doraiswamy, "Estimation of Effective Transport Properties in Packed-Bed Reactors," *Catal. Rev. Sci. Eng.*, **22**(3), 431 (1980).

Kugeler, K., R. Schulten, M. Kugeler, M. Niessen, M. Roth-Kamat, H. Hohn, O. Woike, and J. H. Germer, "The Pebble-Bed–High-Temperature Reactor as a Source of Nuclear Process Heat," **4**, *Kernforschungsanlage Julich*, Jul-1116-RG (1970).

McCabe, W. L., J. C. Smith, and P. Harriot, *Unit Operations of Chemical Engineering*, 4th ed., McGraw-Hill, New York (1985).

McCallister, R. A., "Reformer Employing Finned Heat Pipes," U.S. Pat. No. 4,315,893 (1982).

Parent, Y. O., H. S. Caram, and R. W. Coughlin, "Tube-Wall Catalytic Reactor Cooled by an Annular Heat Pipe," *AIChE J.*, **29**, 443 (1983).

Paripatyadar, S. A., "Cyclic Operation of Sodium Heat Pipe, Solar Reformers," Ph.D. Diss., Dept. Chem. Eng., Univ. Houston (1987).

Paripatyadar, S. A., and J. T. Richardson, "Cyclic Performance of a Heat Pipe, Solar Reformer," to be published.

Rostrup-Nielsen, J. R., "Catalytic Steam Reforming," *Catalysis, Science and Technology*, **5**, J. R. Anderson, M. Boudart, eds., Springer-Verlag, Berlin, 1 (1983).

Shen, J. C., "Dynamics of a Sodium Heat Pipe Natural Gas Reformer," Ph.D. Diss., Dept. Chem. Eng., Univ. Houston (1984).

Van Hook, J. P., "Methane Steam Reforming," *Catal. Rev. Sci. Eng.*, **21**(1), 1 (1980).

Manuscript received Sept. 11, 1987, and revision received Jan. 15, 1988.